Chapter 1

The Nuclear Shell Model

"The fundamental assumption of the shell model [is that] the motion of a single nucleon is governed by a potential representing the average interaction with all the other nucleons."
K. S. Krane

The liquid-drop SEMF (Lectures 4–5) describes bulk binding but cannot explain why certain proton or neutron numbers are especially stable. Just as atomic chemistry is organised by electronic shells, nuclear data show **magic numbers**

$$N, Z = 2, 8, 20, 28, 50, 82, 126 \tag{1.1}$$

at which nuclei are more tightly bound, more abundant, and more spherical than the SEMF alone predicts [6, 14, 1]. The nuclear shell model attributes those gaps to single-particle orbitals in a mean field, completed by a strong spin–orbit force.

1.1 Atomic shells as a guide

In atoms, major shells and subshells organise the periodic table. Closed shells (noble gases) are chemically inert: ionisation energies peak, radii are compact, and valence chemistry is nearly absent. Alkali metals, with a single electron outside a closed shell, share chemical behaviour because that valence electron dominates bonding.

The same logic applies to nuclei, with two important differences. First, both protons and neutrons fill independent sequences of levels (two interpenetrating Fermi seas). Second, the mean field is short-ranged and saturates, so the single-particle spectrum is not hydrogenic. Still, when N or Z reaches a magic number, separation energies jump, radii and abundances show discontinuities, and residual shell effects appear on top of the smooth SEMF [14, 6].

1.2 Empirical evidence for magic numbers

Several independent observables mark shell closures.

Binding-energy residuals. The difference between measured B/A and the SEMF shows positive peaks near magic N or Z (extra binding of closed shells). Pronounced humps appear near $N = 28$, $N = 50$, $N = 82$ and $Z = 28, 50, 82$, among others (Fig. 1.1).

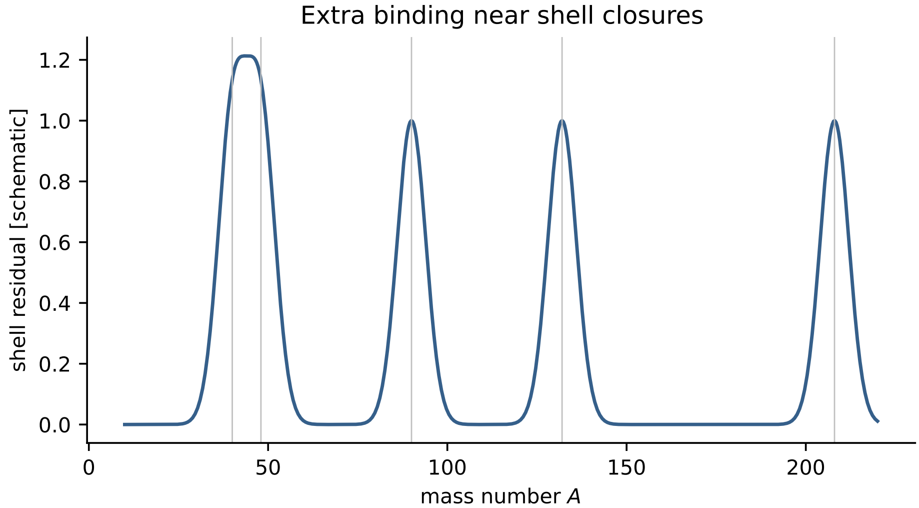

Figure 1.1: Schematic extra-binding residual near shell closures. This vector redraw shows the qualitative signature, not digitized data [1, 6].

Nuclear radii. The ratio of the measured change in nuclear radius to a smooth estimate, when N increases by two, fluctuates near $N = 20, 28, 50, 82$ (Fig. 1.2).

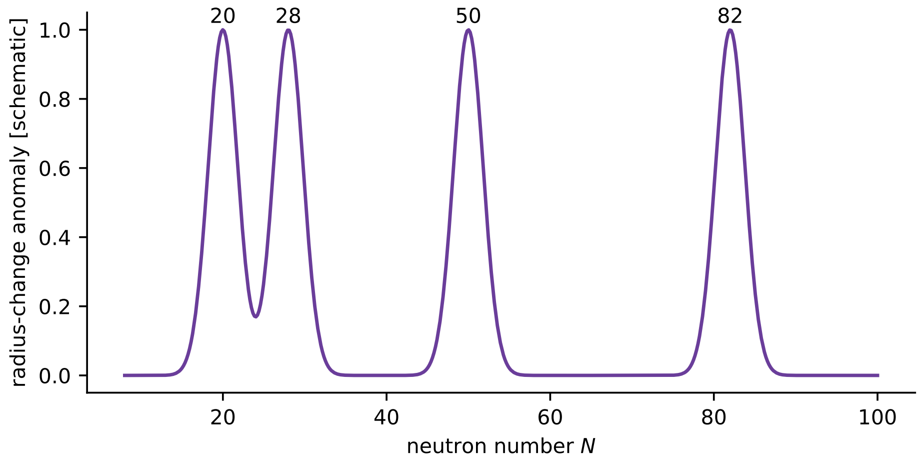

Figure 1.2: Schematic radius-change anomalies near magic neutron numbers; the vector redraw is qualitative rather than a measured dataset [1].

Stable isotones. The number of stable isotones peaks at magic neutron numbers (Fig. 1.3): closed neutron shells favour more proton partners along the valley of stability.

Separation energies and first 2^+. Approaching a closure from below, the last occupied orbit becomes more strongly bound; crossing it, the next nucleon must enter the higher shell. Thus $S_n(N, Z)$ shows a pronounced *downward* step from magic N to $N + 1$, and S_p behaves analogously across magic Z. Equivalently, removing a nucleon from the closed-shell nucleus costs unusually high separation energy. Even–even nuclei near magic numbers also have higher-lying first 2^+ states (more rigid, spherical cores).

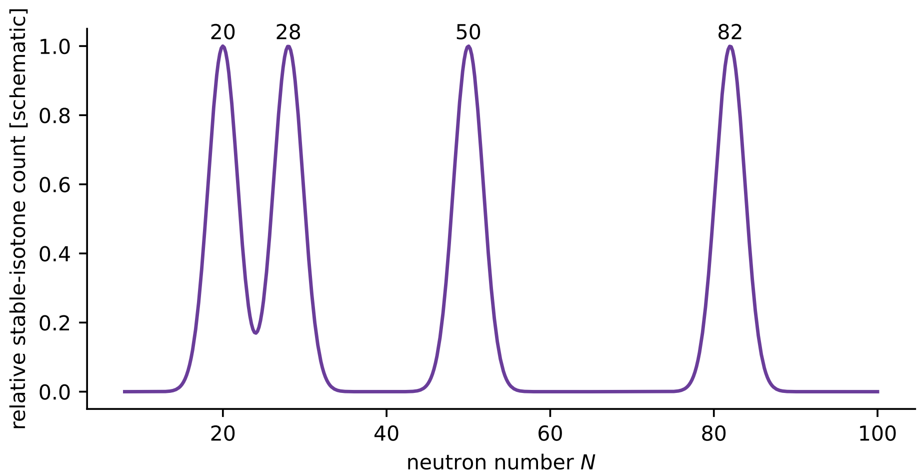

Figure 1.3: Schematic enhancement of stable-isotone counts at magic N. The vector redraw is qualitative rather than a measured dataset [1].

The experimentally identified closures are

$$2,\ 8,\ 20,\ 28,\ 50,\ 82,\ 126.$$

Beyond 126, laboratory superheavy nuclei still show evidence for further shell gaps [6, 1].

Key idea

Magic numbers are experimental facts. The shell model is the mean-field theory that predicts them once a realistic single-particle potential and spin–orbit coupling are chosen.

1.3 Mean field and single-particle motion

The translationally invariant intrinsic Hamiltonian of A nucleons may be written schematically

$$H_{\text{int}} = \sum_{i=1}^{A} \frac{\boldsymbol{p}_i^2}{2m} - \frac{\boldsymbol{P}_{\text{cm}}^2}{2Am} + \sum_{i<j} v_{ij} + \sum_{i<j<k} V_{ijk}, \tag{1.2}$$

where $\boldsymbol{P}_{\text{cm}} = \sum_i \boldsymbol{p}_i$, v_{ij} contains the strong interaction, Coulomb repulsion among protons, and weaker electromagnetic corrections, and V_{ijk} denotes genuine three-nucleon forces discussed in Lecture 11. Subtracting the centre-of-mass (CM) kinetic energy prevents spurious translation of the whole nucleus from being counted as intrinsic excitation. Solving (1.2) exactly is impossible for medium and heavy nuclei. The independent-particle approximation replaces the two-body sum by a one-body mean field $U(\boldsymbol{r})$ that represents the average interaction of one nucleon with all others:

$$H \simeq \sum_{i=1}^{A} \left[\frac{\boldsymbol{p}_i^2}{2m} + U(\boldsymbol{r}_i) \right] + V_{\text{res}}. \tag{1.3}$$

Here V_{res} collects residual two- and three-body effects not absorbed into U. Equation (1.3) also assumes that CM contamination has been removed or is negligible in the chosen intrinsic basis. Pairing and collective correlations live in V_{res} and become essential away from closed shells (Lectures 13–15).

The mean field is not an externally imposed force. It is generated by the nucleons themselves, so a microscopic calculation determines the occupied orbitals and U self-consistently: the orbitals produce a density, the density produces a new field, and the cycle is repeated until both agree. The Pauli principle is essential in this picture. It forces identical nucleons to occupy different quantum states and builds separate proton and neutron Fermi seas. Nuclear saturation then explains why the depth and interior density of the mean field remain roughly independent of A, while its radius grows approximately as $A^{1/3}$.

For spherical nuclei one takes a central potential $U(\boldsymbol{r}) = V(r)$. Spherical symmetry implies that $\boldsymbol{L}^2$ and L_z commute with the single-particle Hamiltonian, so the orbital wave function separates as

$$\psi_{n\ell m}(\boldsymbol{r}) = \frac{u_{n\ell}(r)}{r}\, Y_{\ell m}(\hat{r}). \tag{1.4}$$

Substitute into the single-particle Schrödinger equation

$$-\frac{\hbar^2}{2m}\nabla^2\psi + V(r)\psi = E\psi.$$

The Laplacian in spherical coordinates yields the radial equation for $u(r)$:

$$-\frac{\hbar^2}{2m}\frac{\mathrm{d}^2 u}{\mathrm{d}r^2} + \left[V(r) + \frac{\ell(\ell+1)\hbar^2}{2mr^2}\right]u = E\,u. \tag{1.5}$$

Boundary conditions are

$$u(0) = 0 \qquad \text{(regularity at the origin)} \tag{1.6}$$

and, for a bound state in a finite well,

$$u(r) \to 0 \quad \text{as} \quad r \to \infty. \tag{1.7}$$

Protons and neutrons fill independent sequences of solutions of (1.5) (two Fermi seas). Each spatial orbital of angular momentum ℓ admits $2(2\ell+1)$ identical nucleons once spin $s = \frac{1}{2}$ is included, before spin–orbit coupling is turned on. Different choices of $V(r)$ change level spacings but, without spin–orbit coupling, fail to produce the full set of magic numbers [6, 1, 13].

1.4 Infinite spherical well

Take $V = 0$ for $r < R$ and $V = \infty$ for $r \geq R$. Inside the well the potential term vanishes and (1.5) becomes

$$-\frac{\hbar^2}{2m}\frac{\mathrm{d}^2 u}{\mathrm{d}r^2} + \frac{\ell(\ell+1)\hbar^2}{2mr^2}u = E\,u. \tag{1.8}$$

Define the wave number

$$k = \sqrt{\frac{2mE}{\hbar^2}}, \tag{1.9}$$

so that $E = \hbar^2 k^2/(2m)$. The regular solution of (1.8) is proportional to a spherical Bessel function,

$$u(r) = A\, r\, j_\ell(kr), \tag{1.10}$$

because $j_\ell(\rho)$ satisfies the free radial equation with $\rho = kr$. The infinite wall requires $u(R) = 0$, hence

$$j_\ell(kR) = 0. \tag{1.11}$$

Let $x_{\ell,n}$ denote the nth positive zero of j_ℓ. Then

$$k_{n\ell} = \frac{x_{\ell,n}}{R}, \qquad E_{n\ell} = \frac{\hbar^2 x_{\ell,n}^2}{2mR^2}. \tag{1.12}$$

For $\ell = 0$,

$$j_0(\rho) = \frac{\sin\rho}{\rho},$$

so the zeros are $x_{0,n} = n\pi$ with $n = 1, 2, 3, \ldots$. Higher ℓ require tabulated zeros. Ordering the resulting energies produces the sequence

$$1s,\ 1p,\ 1d,\ 2s,\ 1f,\ 2p,\ 1g,\ \ldots$$

(with $1d$ and $2s$ nearly degenerate in some realisations). Unlike the Coulomb atom, there is no prohibition on $1p$, $1d$, $1f$: the nuclear mean field is not $1/r$.

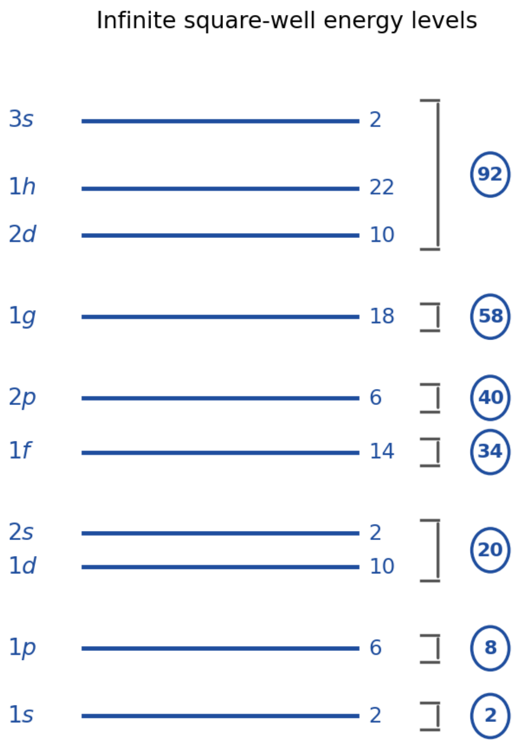

Figure 1.4: Infinite square-well single-particle levels with degeneracies and cumulative shell closures (original lecture figure).

Each spatial orbit of orbital angular momentum ℓ holds $2(2\ell + 1)$ identical nucleons once spin is included: $2\ell+1$ orbital projections and two spin states. Cumulative filling therefore closes shells at

$$\begin{gathered}1s \to 2,\\ 1s+1p \to 2+6=8,\\ 1s+1p+1d+2s \to 8+10+2=20,\end{gathered}$$

but not at 28, 50, 82, 126 [6, 1].

1.5 Isotropic harmonic oscillator

A second standard potential is the three-dimensional isotropic oscillator

$$V(r)=\tfrac{1}{2}m\omega^2r^2. \tag{1.13}$$

In Cartesian coordinates the Hamiltonian is a sum of three independent one-dimensional oscillators,

$$H=\sum_{i=x,y,z}\left(\frac{p_i^2}{2m}+\tfrac{1}{2}m\omega^2x_i^2\right), \tag{1.14}$$

with eigenvalues

$$E=(n_x+n_y+n_z+\tfrac{3}{2})\hbar\omega, \qquad n_x,n_y,n_z=0,1,2,\dots. \tag{1.15}$$

Define the principal oscillator quantum number

$$N=n_x+n_y+n_z=0,1,2,\dots. \tag{1.16}$$

Then

$$E_N=\left(N+\tfrac{3}{2}\right)\hbar\omega. \tag{1.17}$$

Equivalently, in spherical coordinates one writes $N=2n_r+\ell$ with radial quantum number $n_r=0,1,2,\dots$ and orbital angular momentum ℓ. Nuclear spectroscopic labels conventionally shift the radial count so that the lowest s orbit is called $1s$ (corresponding to $n_r=0$).

All states with the same N are degenerate. The number of Cartesian solutions with $n_x+n_y+n_z=N$ is

$$\binom{N+2}{2}=\frac{(N+1)(N+2)}{2}. \tag{1.18}$$

Including two spin projections multiplies by 2, so the occupancy of major shell N is

$$g_N=(N+1)(N+2). \tag{1.19}$$

Explicitly:

N	Orbitals (nuclear labels)	Occupancy g_N	Cumulative
0	$1s$	2	2
1	$1p$	6	8
2	$1d, 2s$	12	20
3	$1f, 2p$	20	40
4	$1g, 2d, 3s$	30	70

Cumulative magic numbers from pure oscillator filling are therefore $2, 8, 20, 40, 70, \ldots$. Again the empirical sequence beyond 20 is missed [6, 14, 13].

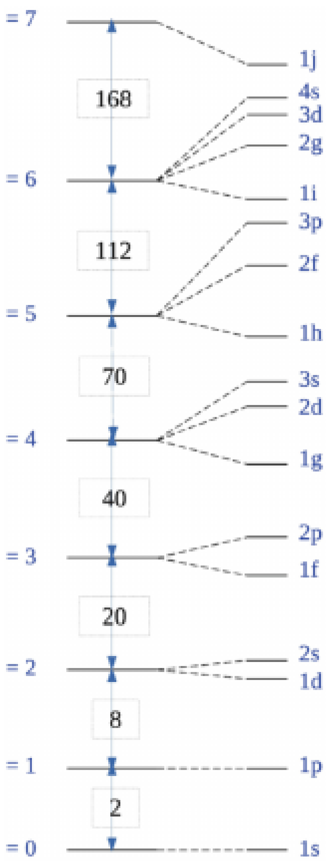

Figure 1.5: Harmonic-oscillator major shells with cumulative occupancies (original lecture figure).

Remark

Both the infinite well and the oscillator are unphysical as absolute walls: a particle cannot be removed by any finite energy. Real nuclei have finite separation energies $S_n, S_p \sim$ a few to tens of MeV. Finite wells (Lecture 13) fix that defect without, by themselves, fixing the magic numbers past 20.

1.6 Toward a realistic potential: Woods–Saxon shape

A finite square well allows a nucleon to have finite removal (separation) energy but retains a discontinuous edge. Nuclear density falls smoothly over a 10%–90% surface thickness $t = 4a \ln 3$, typically 2–3 fm. The most successful central mean field is the Woods–Saxon form

$$V(r) = -\frac{V_0}{1 + \exp[(r - R)/a]}, \tag{1.20}$$

with $R = r_0 A^{1/3}$ and diffuseness $a \sim 0.5$ fm (Fig. 1.6). Even so, Woods–Saxon alone does not rearrange the magic numbers past 20; the essential missing piece is spin–orbit coupling [10, 6].

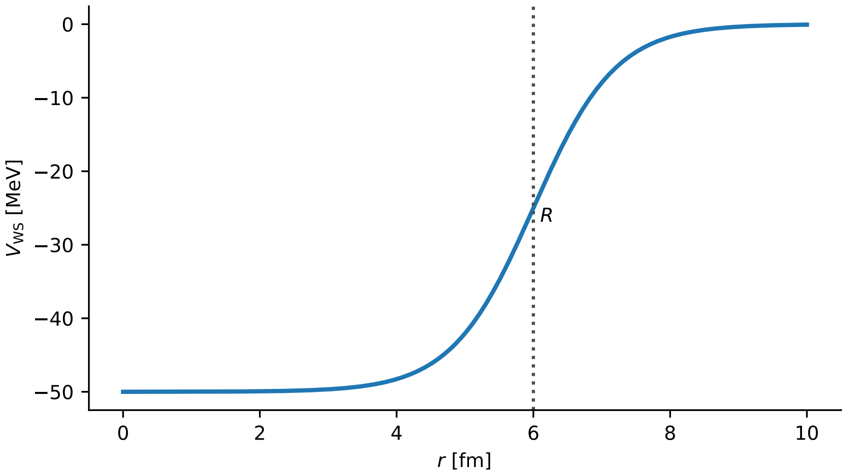

Figure 1.6: Woods–Saxon single-particle potential: flat attractive interior, diffuse surface, and finite depth (original vector evaluation of the analytic form; Woods and Saxon [10]).

1.7 Spin–orbit coupling and the correct magic numbers

Historical note: Mayer and Jensen (1949)

Maria Goeppert Mayer and, independently, **J. Hans D. Jensen** (with Haxel and Suess) showed that a strong nuclear spin–orbit force $V_{\mathrm{so}}(r)\, \boldsymbol{\ell} \cdot \boldsymbol{s}$ splits each $\ell > 0$ level into $j = \ell \pm \frac{1}{2}$ and rearranges the spectrum so that the empirical magic numbers appear. They shared the 1963 Nobel Prize in Physics with Wigner. The nuclear spin–orbit force is much stronger than its atomic electromagnetic counterpart and is a residual effect of the underlying NN interaction [6, 14].

Without spin–orbit coupling the single-particle Hamiltonian commutes with ℓ_z and s_z. A dimensionally explicit phenomenological choice is

$$H_{\mathrm{so}} = C_{\mathrm{so}} \frac{1}{r} \frac{\mathrm{d}V_{\mathrm{WS}}}{\mathrm{d}r} \frac{\boldsymbol{\ell} \cdot \boldsymbol{s}}{\hbar^2}, \tag{1.21}$$

where C_{so} has dimensions of length squared; hence $(1/r)\mathrm{d}V/\mathrm{d}r$ times C_{so} has dimensions of energy. Because V_{WS} changes most rapidly near $r \simeq R$, the nuclear spin–orbit interaction is surface peaked. High-ℓ orbits are especially sensitive: their centrifugal barrier pushes their probability density toward the surface, precisely where the derivative is largest. The constant and its sign are fitted so that the $j = \ell + \frac{1}{2}$ partner is the lower one. With this term, the good quantum numbers change: H no longer commutes with ℓ_z or s_z, but still commutes with ℓ^2, s^2, $\boldsymbol{j}^2$ and j_z, where

$$\boldsymbol{j} = \boldsymbol{\ell} + \boldsymbol{s}, \qquad j = \ell \pm \tfrac{1}{2} \quad (\ell \geq 1). \tag{1.22}$$

States are therefore labelled $n\ell_j$ (e.g. $1d_{5/2}$, $1d_{3/2}$).

1.7.1 Expectation value of the spin–orbit operator

Start from the operator identity obtained by expanding $\boldsymbol{j}^2 = (\boldsymbol{\ell} + \boldsymbol{s})^2$:

$$\boldsymbol{j}^2 = \boldsymbol{\ell}^2 + \boldsymbol{s}^2 + 2\,\boldsymbol{\ell} \cdot \boldsymbol{s}, \tag{1.23}$$

and therefore

$$\boldsymbol{\ell} \cdot \boldsymbol{s} = \frac{1}{2}(\boldsymbol{j}^2 - \boldsymbol{\ell}^2 - \boldsymbol{s}^2). \tag{1.24}$$

On a simultaneous eigenstate of $\boldsymbol{j}^2$, $\boldsymbol{\ell}^2$ and $\boldsymbol{s}^2$ with eigenvalues $j(j+1)\hbar^2$, $\ell(\ell+1)\hbar^2$ and $s(s+1)\hbar^2$,

$$\langle \boldsymbol{\ell} \cdot \boldsymbol{s} \rangle = \frac{\hbar^2}{2}\big[j(j+1) - \ell(\ell+1) - s(s+1)\big]. \tag{1.25}$$

For nucleons $s = \frac{1}{2}$, so $s(s+1) = \frac{3}{4}$.

Partner $j = \ell + \frac{1}{2}$.

$$j(j+1) = \left(\ell + \tfrac{1}{2}\right)\left(\ell + \tfrac{3}{2}\right) = \ell^2 + 2\ell + \tfrac{3}{4},$$

hence

$$j(j+1) - \ell(\ell+1) - s(s+1) = (\ell^2 + 2\ell + \tfrac{3}{4}) - (\ell^2 + \ell) - \tfrac{3}{4} = \ell,$$

and

$$\langle \boldsymbol{\ell} \cdot \boldsymbol{s} \rangle_{j=\ell+1/2} = \frac{\hbar^2}{2}\,\ell. \tag{1.26}$$

Partner $j = \ell - \frac{1}{2}$.

$$j(j+1) = \left(\ell - \tfrac{1}{2}\right)\left(\ell + \tfrac{1}{2}\right) = \ell^2 - \tfrac{1}{4},$$

hence

$$j(j+1) - \ell(\ell+1) - s(s+1) = (\ell^2 - \tfrac{1}{4}) - (\ell^2 + \ell) - \tfrac{3}{4} = -(\ell+1),$$

and

$$\langle \boldsymbol{\ell} \cdot \boldsymbol{s} \rangle_{j=\ell-1/2} = -\frac{\hbar^2}{2}\,(\ell+1). \tag{1.27}$$

Treating $H_{\rm so}$ as a first-order perturbation to a central-field radial state $u_{n\ell}$, normalized by $\int_0^\infty |u_{n\ell}(r)|^2 \mathrm{d}r = 1$, gives

$$\Delta E^{(1)}_{n\ell j} = C_{\rm so} \int_0^\infty |u_{n\ell}(r)|^2 \frac{1}{r}\frac{\mathrm{d}V_{\rm WS}}{\mathrm{d}r}\,\mathrm{d}r\,\frac{\langle \boldsymbol{\ell} \cdot \boldsymbol{s} \rangle_j}{\hbar^2}. \tag{1.28}$$

Defining the energy coefficient multiplying $\langle \boldsymbol{\ell} \cdot \boldsymbol{s} \rangle$ as $\langle f \rangle$, the nuclear ordering corresponds to $\langle f \rangle < 0$, so the $j = \ell + \frac{1}{2}$ partner is lowered and the $j = \ell - \frac{1}{2}$ partner is raised. Their splitting is

$$\Delta E_{\text{so}} = E_{j=\ell-1/2} - E_{j=\ell+1/2} = -\langle f \rangle \, \frac{\hbar^2}{2} \, (2\ell + 1). \tag{1.29}$$

Large-ℓ orbits therefore split most; s states ($\ell = 0$) do not split at all.

That reordering is decisive. The high-j members of each major shell ($1f_{7/2}$, $1g_{9/2}$, $1h_{11/2}$, $1i_{13/2}$) drop into lower major shells and open gaps at the observed magic numbers [16, 17, 6, 14]:

- $1f_{7/2}$ (occupancy $2j + 1 = 8$) alone closes a shell at $20 + 8 = 28$;
- after 28, filling $2p_{3/2}(4) + 1f_{5/2}(6) + 2p_{1/2}(2) + 1g_{9/2}(10) = 22$ yields $28 + 22 = 50$;
- the next major regrouping, including $1h_{11/2}$ (occupancy 12), yields 82;
- including $1i_{13/2}$ (occupancy 14) yields 126.

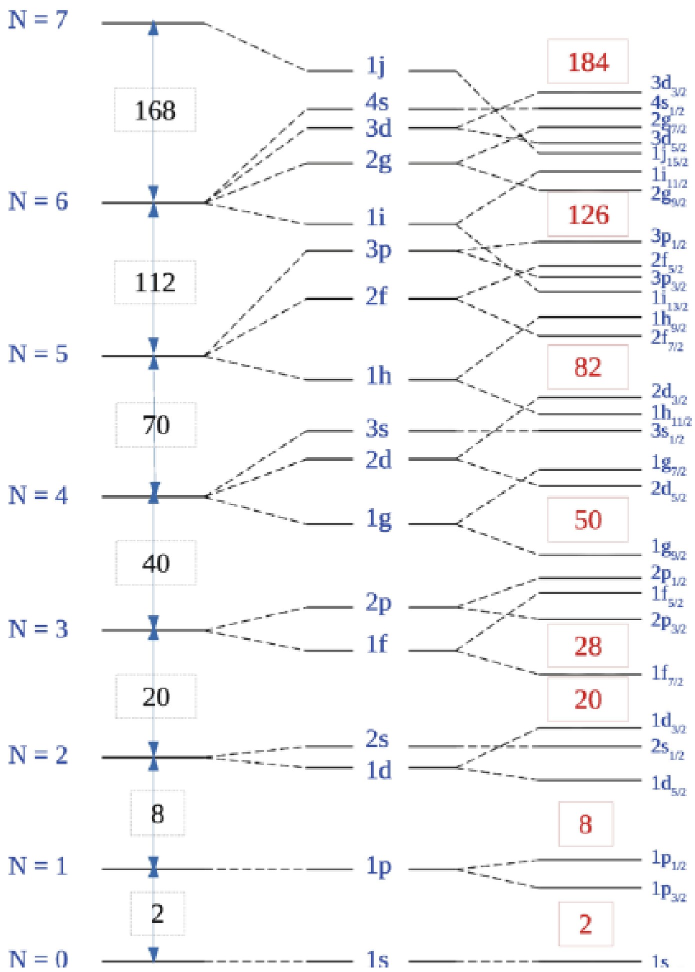

Figure 1.7: Harmonic-oscillator levels with ℓ^2 and spin–orbit splitting. Empirical magic numbers are highlighted (original lecture figure; cf. Mayer [16] and Haxel, Jensen and Suess [17]).

Each j subshell holds $2j + 1$ identical nucleons (protons or neutrons separately). Cumulative filling:

Newly added subshell(s)	Total occupancy N or Z
$1s_{1/2}$	2
$+1p_{3/2}, 1p_{1/2}$	8
$+1d_{5/2}, 2s_{1/2}, 1d_{3/2}$	20
$+1f_{7/2}$	28
$+2p_{3/2}, 1f_{5/2}, 2p_{1/2}, 1g_{9/2}$	50
$+1g_{7/2}, 2d_{5/2}, 2d_{3/2}, 3s_{1/2}, 1h_{11/2}$	82
$+1h_{9/2}, 2f_{7/2}, \ldots, 1i_{13/2}$	126

Key idea

Central potentials alone give $2, 8, 20$. Spin–orbit coupling is required for $28, 50, 82, 126$. Remember the mechanism, not only the list: surface-peaked spin–orbit coupling lowers the high-j ($j = \ell + \frac{1}{2}$) orbit, that orbit carries $2j + 1$ nucleons, and its large occupancy creates the next shell gap.

Caution

Nuclear spin–orbit ordering is opposite to the atomic fine-structure pattern for electrons: in nuclei $j = \ell + \frac{1}{2}$ lies *below* $j = \ell - \frac{1}{2}$. The strength is also orders of magnitude larger (MeV scale vs. fractions of an eV in atoms), because the force is residual strong interaction, not electromagnetism.

1.8 Why the potential shape alone is not enough

Finite square wells, wells with rounded edges, and the Woods–Saxon form all improve separation energies and level densities relative to infinite walls. They do *not*, by themselves, produce the full magic sequence: the level order remains close to that of the oscillator or infinite well until $\boldsymbol{\ell} \cdot \boldsymbol{s}$ is added. Conversely, once a strong spin–orbit term is present, magic numbers appear for a wide class of reasonable central shapes. The empirical gaps are therefore a robust signature of spin–orbit physics, not a fine-tuned accident of one potential [6, 1].

1.9 Deeper physics: harmonic-oscillator shells and spin–orbit splitting

1.9.1 HO quantum numbers and naive closures

In a three-dimensional harmonic oscillator,

$$E_N = \hbar\omega\left(N + \frac{3}{2}\right), \qquad N = 2n_r + \ell, \tag{1.30}$$

with radial quantum number n_r and orbital ℓ. Degenerate shells at $N = 0, 1, 2, 3, \ldots$ would give closures at 2, 6, 12, 20 nucleons if all ℓ values up to N were filled with their full degeneracies $(2\ell + 1) \times 2$ (spin). That pattern matches the first two magic numbers (2 and 8) but fails at 20:

experiment demands 20, 28, 50, 82, 126 [6, 1].

1.9.2 Spin–orbit splitting in one formula

A nucleon with velocity $\boldsymbol{v}$ in orbit ℓ sees a magnetic field from the nuclear centre, and Thomas precession fixes the single-particle spin–orbit potential to the form

$$\hat{H}_{\text{so}} = -f(r)\,\boldsymbol{L}\cdot\boldsymbol{S}, \tag{1.31}$$

with $f(r) > 0$ in the nuclear interior. States with $j = \ell + \frac{1}{2}$ ($\boldsymbol{L}$ and $\boldsymbol{S}$ aligned) are pushed *down*; states with $j = \ell - \frac{1}{2}$ are pushed *up*. The $1f_{7/2}$ orbit dropping below $2p_{3/2}$ at $N = 28$ is the canonical example: without (1.31), the shell at $N = 20$ would close too early.

Splitting scale estimate

Take $\hbar\omega \approx 41\,A^{-1/3}$ MeV and a typical $f(r) \sim 10$ MeV acting on $\langle \boldsymbol{L}\cdot\boldsymbol{S}\rangle \sim \ell/2$ for $j = \ell + \frac{1}{2}$. The resulting ~ 5–10 MeV splittings between $j = \ell \pm \frac{1}{2}$ partners are comparable to the HO spacing and suffice to reorder levels across major shells. Magic numbers are therefore not a property of HO alone but of HO plus a strong spin–orbit force (Mayer and Jensen, 1949) [6, 14].

Remark

Limits. The HO picture ignores deformation (Lecture 15), pairing gaps, and configuration mixing. Far from stability, traditional closures migrate (islands of inversion). The filling diagram in the main text is a mean-field map: residual interactions spread single-particle strength and shift separation energies by hundreds of keV even near closed shells.

1.9.3 Magic numbers as discontinuities in observables

Each magic number appears simultaneously in:

- a jump in two-nucleon separation energy S_{2n} (Section 1.10);
- a peak in the first 2^+ energy in even–even neighbours (Lecture 15, **??**);
- a reduction in collectivity (small $B(E2)$ near closed cores).

The HO plus spin–orbit model predicts *where* those discontinuities occur; residual interactions set their *size*. Filling the WS diagram (Lecture 13) is the operational step that turns magic numbers into I^π and Schmidt assignments (Lecture 14) [1, 6].

1.9.4 Pairing and even–even 0^+ ground states

Even–even nuclei have $I^\pi = 0^+$ because like nucleons pair to $J = 0$ (**??**). Pairing gaps of ~ 1 MeV smooth odd–even staggering in separation energies but do not remove magic-number jumps at major shells. The shell model therefore uses a mean field (this lecture) plus pairing (later refinements) before configuration mixing and collectivity (Lecture 15) enter [14, 6].

1.9.5 Harmonic-oscillator frequency $\hbar\omega$

The empirical rule $\hbar\omega \approx 41\, A^{-1/3}\,\mathrm{MeV}$ sets the spacing between major HO shells and therefore the scale of separation-energy jumps at magic numbers. For ^{208}Pb, $\hbar\omega \approx 7\,\mathrm{MeV}$, comparable to the spin–orbit splitting of the $1i_{13/2}$ and $2g_{9/2}$ orbitals near the neutron drip line. Residual interactions of similar magnitude mix those orbits in exotic nuclei, which is why the independent-particle picture weakens far from stability even when magic numbers persist in lighter isotopes [1, 6].

1.10 Further physics: separation energies and double magic nuclei

Doubly magic nuclei (Z and N both magic), such as ^{4}He, ^{16}O, ^{40}Ca, ^{48}Ca, and ^{208}Pb, combine large S_n and S_p, spherical shape, and simple particle/hole spectra when one nucleon is added or removed [14, 6, 20]. They are the benchmarks against which residual interactions and ab initio methods are tested.

The one-nucleon separation energies

$$S_n(A,Z) = B(A,Z) - B(A-1,Z), \tag{1.32}$$
$$S_p(A,Z) = B(A,Z) - B(A-1,Z-1) \tag{1.33}$$

jump when a shell closes, in direct analogy with atomic ionisation energies. Two-nucleon separation energies S_{2n} and S_{2p} are often smoother against odd–even staggering and therefore especially useful for mapping shell evolution far from stability.

Magic numbers need not be universal. Far from the valley of β stability, especially in neutron-rich light and medium-mass nuclei, experimental spectroscopy shows that traditional closures such as $N = 20$ or $N = 28$ can weaken or migrate ("islands of inversion"). The next predicted closures beyond $N = 126$ (e.g. $N = 184$, $Z = 114$ or nearby) underlie the search for superheavy islands of stability [14, 1].

1.10.1 HO filling through $N = 40$ and where it fails

In the pure HO model (Equation (1.30)), each major shell N contains orbits with $\ell = N, N-2, \ldots$ up to parity constraints. Counting degeneracies $(2\ell + 1) \times 2$ and accumulating:

N	Orbits	Cumulative nucleons	Experiment
0	$1s_{1/2}$	2	2
1	$1p_{3/2}, 1p_{1/2}$	6	6
2	$1d_{5/2}, 2s_{1/2}, 1d_{3/2}$	12	—
3	$1f_{7/2}, \ldots$	20 (HO)	20
with spin–orbit: $1f_{7/2}$ drops $\rightarrow$ magic 28			

The failure at $N = 2$ (HO predicts 12, magic is 8) is cured by spin–orbit pushing $1p_{3/2}$ down from the $N = 2$ shell. The failure at 20 without spin–orbit is cured by $1f_{7/2}$ dropping to open the gap at 28 [6, 1].

1.10.2 Spin–orbit splittings in the WS spectrum

In a Woods–Saxon plus spin–orbit potential (Lecture 13), the splitting between $j = \ell + \frac{1}{2}$ and $j = \ell - \frac{1}{2}$ partners is largest for high ℓ near the surface, where $f(r)$ peaks. The $1f_{7/2}$ orbital ($\ell = 3$) experiences a $\sim 7\,\text{MeV}$ downward shift relative to its $j = \ell - \frac{1}{2}$ partner, enough to reorder the $N = 3$ shell. Without this term, magic numbers would stop at 20 and the periodic table of nuclei would not exist in its observed form [6, 14].

Shell gap vs $\hbar\omega$

For ^{40}Ca, the proton separation energy jump across $Z = 20$ is $\Delta S_p \sim 15\,\text{MeV}$, while typical single-particle spacings within a major shell are $\sim$ 1–3 MeV. The gap is therefore an order of magnitude larger than the residual interaction scale, justifying the independent-particle picture for one nucleon outside ^{40}Ca (Lecture 13).

1.10.3 Bridge to Lectures 13–15

The filling diagram derived here supplies the orbit labels for I^π assignments (Lecture 13) and Schmidt moments (Lecture 14). Mid-shell even–even nuclei violate the independent-particle picture for $E(2^+)$ (Lecture 15): the same shell gaps that produce magic numbers also control when collectivity turns on. Separation-energy jumps at magic N (Section 1.10) are the experimental signature that the HO plus spin–orbit map captures the mean field [1, 20].

1.10.4 Two-nucleon separation energies near ^{40}Ca

The quantity $S_{2n}(A, Z) = B(A, Z) - B(A - 2, Z)$ smooths odd–even pairing staggering and highlights shell closures. For the calcium chain, S_{2n} shows pronounced steps at $N = 20$ and $N = 28$, matching the WS filling diagram (**??**). Mid-shell between closures, S_{2n} falls and $E(2^+)$ in even–even neighbours drops (Lecture 15), marking the onset of collectivity. Magic numbers are therefore visible simultaneously in separation energies, radii (Figure 1.2), and excited-state systematics [6, 1].

1.11 Deeper reading: magic numbers, spin–orbit, and migration

The harmonic-oscillator magic numbers $2, 8, 20, 40, \ldots$ fail above ^{40}Ca without a strong spin–orbit splitting that produces $28, 50, 82, 126$. In neutron-rich nuclei those closures can migrate or disappear (islands of inversion), while new closures appear. The tensor force of Lecture 9 is one microscopic driver; continuum coupling near drip lines is another (Lecture 13).

Ab initio valence-space methods now derive effective interactions from chiral Hamiltonians rather than fitting only two-body matrix elements to spectra. When comparing a textbook USD-type interaction with an ab initio valence Hamiltonian, ask which observables were used in the fit or validation and how uncertainties are quoted. Magic numbers remain the organisational map; they are no longer immutable integers.

Spin–orbit energy scale

A spin–orbit splitting of several mega-electronvolts near the Fermi surface reshuffles oscillator shells into the empirical magic sequence. Without it, ^{48}Ca and ^{208}Pb would not be doubly magic in the textbook sense. Measuring single-particle energies with transfer reactions (Lecture 21) is how those splittings are tracked into exotic isotopes.

Effective interactions

Phenomenological valence interactions encode core polarisation in fitted two-body matrix elements. Ab initio valence-space methods compute those effects from a parent Hamiltonian. When spectra agree but charge radii disagree, the operator (effective charge) is usually the culprit, not the energies alone (Lecture 14–15 themes).

Filling diagram audit

Reproduce the oscillator filling through $N = 40$ and then insert spin–orbit splitting to recover $28, 50, 82$. Mark which empirical magic numbers require the spin–orbit step. Next, list three nuclei often cited as islands of inversion and write one sentence each on the spectroscopic evidence (low $E(2^+)$, large $B(E2)$, or intruder configurations). That audit turns magic numbers from memorised integers into falsifiable claims.

When reading an ab initio spectrum for a medium-mass nucleus, record the chiral order, many-body method, and model-space truncation in a three-line note. Without those, a predicted gap cannot be compared fairly to experiment or to a phenomenological shell-model fit. Lectures 13–15 then test the resulting single-particle and collective consequences.

Magic numbers are experimental claims with theoretical mechanisms. Spin–orbit coupling, tensor forces, and continuum effects are the mechanisms this course emphasises.

In practice, rework one numerical estimate from the lecture with a different parameter set and compare the shift to the quoted experimental uncertainty. If the shift exceeds the uncertainty, the estimate is teaching a scale, not delivering a fit. That distinction keeps theoretical cartoons honest when they sit beside evaluated data tables and modern many-body calculations. Along the course arc, write one sentence linking this chapter backward and one forward: the discipline of those two sentences is as important as any single formula. Examination problems rarely ask for a literature review, but they do ask for the scale argument that literature reviews presuppose.

Synthesis problem

Write a half-page note that (i) restates the chapter's central scale or selection rule in one equation, (ii) evaluates it numerically for one concrete nucleus or energy, and (iii) names the neighbouring lecture that uses the result. Keep the note free of research-frontier speculation; the goal is fluency with the lecture physics itself. If an assumption fails (Born approximation, spherical mean field, allowed transition, one-dimensional barrier), state the failure mode in a final sentence. That habit converts passive reading into examination-ready understanding and makes the later research-frontier box read as an extension rather than a replacement.

Research frontier: ab initio shells and student projects

Magic numbers of Lecture 12 are no longer viewed as immutable integers carved into the chart of nuclides. In neutron-rich nuclei, traditional closures migrate or disappear ("islands of inversion"), while new closures appear; the tensor force and continuum coupling are key microscopic drivers [43]. Ab initio methods (coupled cluster, IMSRG, and valence-space IMSRG) now compute medium-mass nuclei from chiral Hamiltonians and derive effective shell-model interactions microscopically rather than by purely phenomenological fits [44, 51]. What remains uncertain is the quantitative accuracy of ab initio spectra near open-shell nuclei where collective correlations are strong, and how to assign meaningful theory-uncertainty bars when truncating the many-body expansion. Facility programmes at rare-isotope laboratories are designed to test these predictions with transfer, knockout, and γ-ray spectroscopy far from stability [52].

Students reading ab initio papers should look for three reported items: the chiral order of the Hamiltonian, the many-body truncation, and a quantified uncertainty estimate. Without those, a predicted magic gap is difficult to compare with experiment. The lecture filling diagram remains the map against which those predictions are judged.

Comparing two published IMSRG or coupled-cluster gap predictions for the same nucleus, with their stated truncations, is a useful student literature exercise.

Facility proposals increasingly ask for such theory-uncertainty statements before claiming a new closure has been established.

Student directions. (1) Table exercise: reproduce the oscillator filling table through $N = 40$ and mark where experiment disagrees. (2) Case study: pick one island-of-inversion nucleus (e.g. ^{32}Mg) and summarise the spectroscopic evidence for a weakened $N = 20$ gap. (3) Short essay: contrast phenomenological USD-type interactions with a valence-space IMSRG Hamiltonian.

1.12 Problems with solutions

Problem 12.1 — Occupancy of a j subshell

How many identical nucleons can occupy a $1g_{9/2}$ orbit? What cumulative magic number is completed when $1g_{9/2}$ is filled after the $N = 28$ core and the $2p_{3/2}, 1f_{5/2}, 2p_{1/2}$ subshells?

Problem 12.5 — CM subtraction and separation step

Why is $\boldsymbol{P}_{\rm cm}^2/(2Am)$ subtracted from the many-body Hamiltonian? Also state the expected direction of the one-neutron separation energy step when going from a magic-N isotope to its $N + 1$ neighbour.

Solution 12.5

The subtraction removes kinetic energy of translating the nucleus as a whole, leaving only intrinsic motion; otherwise spurious CM excitations can pollute the shell spectrum. The first neutron above a closed shell occupies a higher, less-bound orbital, so S_n drops from magic N to $N+1$. Conversely, removing a neutron from the closed-shell nucleus requires an unusually large S_n [6, 1].

Solution 12.1

A j subshell holds $2j+1$ identical nucleons, so

$$2j+1 = 2 \cdot \tfrac{9}{2} + 1 = 10.$$

After the $N = 28$ core the next orbits fill as

$$\begin{aligned} 2p_{3/2} &: \ 4, \\ 1f_{5/2} &: \ 6, \\ 2p_{1/2} &: \ 2, \\ 1g_{9/2} &: \ 10, \end{aligned}$$

for a total of $4+6+2+10 = 22$. The cumulative closure is $28+22 = 50$ [6, 16].

Problem 12.2 — Why HO misses magic 28

The isotropic oscillator produces closures at $2, 8, 20, 40, \ldots$. Explain in one or two sentences how spin–orbit coupling creates a gap at 28.

Solution 12.2

In the $N = 3$ oscillator shell the spin–orbit term lowers $1f_{7/2}$ ($j = \ell + \frac{1}{2}$, $\ell = 3$) below the remaining $2p$ and $1f_{5/2}$ partners. The isolated $1f_{7/2}$ subshell holds $2j+1 = 8$ nucleons, so a new gap opens at $20+8 = 28$ [6, 14, 17].

Problem 12.3 — $\ell \cdot s$ expectation values

Using $\boldsymbol{\ell} \cdot \boldsymbol{s} = \frac{1}{2}(\boldsymbol{j}^2 - \boldsymbol{\ell}^2 - \boldsymbol{s}^2)$, show that $\langle \boldsymbol{\ell} \cdot \boldsymbol{s} \rangle = \frac{1}{2}\ell\hbar^2$ for $j = \ell + \frac{1}{2}$ and $-\frac{1}{2}(\ell+1)\hbar^2$ for $j = \ell - \frac{1}{2}$. Then show that the partner splitting is proportional to $2\ell+1$.

Solution 12.3

With $s = \frac{1}{2}$, $s(s+1) = \frac{3}{4}$. For $j = \ell + \frac{1}{2}$,

$$j(j+1) = \left(\ell + \tfrac{1}{2}\right)\left(\ell + \tfrac{3}{2}\right) = \ell^2 + 2\ell + \tfrac{3}{4},$$

so

$$j(j+1) - \ell(\ell+1) - s(s+1) = \ell$$

and $\langle \boldsymbol{\ell} \cdot \boldsymbol{s} \rangle = \frac{1}{2}\ell\hbar^2$. For $j = \ell - \frac{1}{2}$,

$$j(j+1) - \ell(\ell+1) - s(s+1) = -(\ell+1),$$

hence $-\frac{1}{2}(\ell+1)\hbar^2$. The difference of the two expectation values is $\frac{1}{2}(2\ell+1)\hbar^2$, so the energy splitting scales as $2\ell+1$ once $\langle f(r)\rangle$ is factored out [6, 13].

Problem 12.4 — Oscillator degeneracy

Derive the occupancy $g_N = (N+1)(N+2)$ of major shell N in the isotropic three-dimensional oscillator, including spin.

Solution 12.4

The number of non-negative integer solutions of $n_x+n_y+n_z = N$ is $\binom{N+2}{2} = (N+1)(N+2)/2$. Each spatial state admits two spin projections, so

$$g_N = 2 \cdot \frac{(N+1)(N+2)}{2} = (N+1)(N+2).$$

For $N = 0, 1, 2, 3$ one recovers $2, 6, 12, 20$, and the cumulative closures $2, 8, 20, 40$ [6, 1].

Bibliography

[1] R. A. Dunlap, *An Introduction to the Physics of Nuclei and Particles* (2nd ed.), IOP Publishing, Bristol (2023), DOI: 10.1088/978-0-7503-6094-4, Ch. 3 (Nuclear composition and size).

[2] W. Demtröder, *Nuclear and Particle Physics*, Undergraduate Lecture Notes in Physics, Springer, Cham (2023).

[3] S. Petrera, *Problems and Solutions in Nuclear and Particle Physics*, UNITEXT for Physics, Springer, Cham (2019).

[4] F. Terranova, *A Modern Primer in Particle and Nuclear Physics*, Oxford University Press (2021).

[5] S. D'Auria, *Introduction to Nuclear and Particle Physics*, Undergraduate Lecture Notes in Physics, Springer, Cham (2018).

[6] K. S. Krane, *Introductory Nuclear Physics*, Wiley, New York (1988).

[7] R. Hofstadter, "Electron scattering and nuclear structure," Rev. Mod. Phys. **28**, 214 (1956).

[8] H. F. Ehrenberg, R. Hofstadter, U. Meyer-Berkhout, D. G. Ravenhall, and S. E. Sobottka, "High-Energy Electron Scattering and the Charge Distribution of Carbon-12 and Oxygen-16," Phys. Rev. **113**, 666 (1959).

[9] H. Yukawa, "On the interaction of elementary particles. I," Proc. Phys.-Math. Soc. Japan **17**, 48 (1935).

[10] R. D. Woods and D. S. Saxon, "Diffuse surface optical model for nucleon-nuclei scattering," Phys. Rev. **95**, 577 (1954).

[11] H. G. J. Moseley, "The high-frequency spectra of the elements," Phil. Mag. **26**, 1024 (1913); **27**, 703 (1914).

[12] C. F. von Weizsäcker, "Zur Theorie der Kernmassen," Z. Phys. **96**, 431 (1935).

[13] P. Cappellaro, *Introduction to Applied Nuclear Physics* (MIT OpenCourseWare / LibreTexts), CC BY-NC-SA 4.0.

[14] J.-L. Basdevant, J. Rich, and M. Spiro, *Fundamentals in Nuclear Physics: From Nuclear Structure to Cosmology*, Springer, New York (2005).

[15] D. Tong, *Particle Physics*, Lecture notes (University of Cambridge / CERN school notes).

[16] M. G. Mayer, "On closed shells in nuclei. II," Phys. Rev. **75**, 1969 (1949).

[17] O. Haxel, J. H. D. Jensen, and H. E. Suess, "On the "magic numbers" in nuclear structure," Phys. Rev. **75**, 1766 (1949).

[18] T. Schmidt, "Über die magnetischen Momente der Atomkerne," Z. Phys. **106**, 358 (1937).

[19] L. W. Nordheim, "On spins, moments, and shells in nuclei," Phys. Rev. **78**, 294 (1950).

[20] Evaluated Nuclear Structure Data File (ENSDF), National Nuclear Data Center, Brookhaven National Laboratory, `https://www.nndc.bnl.gov/ensdf/`.

[21] NuDat 3, National Nuclear Data Center, Brookhaven National Laboratory, `https://www.nndc.bnl.gov/nudat3/`.

[22] N. J. Stone, "Table of nuclear magnetic dipole and electric quadrupole moments," At. Data Nucl. Data Tables **90**, 75 (2005); updated compilations at NNDC.

[23] W. N. Cottingham and D. A. Greenwood, *An Introduction to Nuclear Physics* (2nd ed.), Cambridge University Press, Cambridge (2001).

[24] H. Geiger and J. M. Nuttall, "The ranges of the α particles from the radioactive substances," Phil. Mag. **22**, 613 (1911).

[25] G. Gamow, "Zur Quantentheorie des Atomkernes," Z. Phys. **51**, 204 (1928).

[26] R. W. Gurney and E. U. Condon, "Wave mechanics and radioactive disintegration," Nature **122**, 439 (1928); Phys. Rev. **33**, 127 (1929).

[27] M. Wang, W. J. Huang, F. G. Kondev, G. Audi, and S. Naimi, "The AME 2020 atomic mass evaluation (II). Tables, graphs and references," Chin. Phys. C **45**, 030003 (2021).

[28] Laboratoire National Henri Becquerel (LNHB), Recommended decay data, `http://www.lnhb.fr/nuclear-data/nuclear-data-table/`.

[29] L. M. Langer, R. D. Moffat, and H. C. Price, Jr., "Low energy beta-ray spectra: P^{32} and Cu^{64}," Phys. Rev. **76**, 1725 (1949).

[30] L. M. Langer and H. C. Price, Jr., "Shapes of the beta-spectra of the forbidden transitions of Sb^{124}, Rb^{86}, Sr^{89}, Y^{91}, and Cs^{137}," Phys. Rev. **75**, 1769 (1949).

[31] D. C. Camp and L. M. Langer, "The shape of the ^{66}Ga positron spectrum and the contribution from $0^+ \to 0^+$ transitions," Phys. Rev. **129**, 1782 (1963).

[32] H. C. Verma, *Nuclear Physics: Fundamentals and Applications*, NPTEL/IIT Kanpur lecture series, `https://hcverma.in/ncl_phy_lectures`.

[33] International Atomic Energy Agency, *LiveChart of Nuclides*, evaluated structure, decay, reaction, and fission-yield data, `https://www-nds.iaea.org/relnsd/vcharthtml/VChartHTML.html`.

[34] T. Kibédi, T. W. Burrows, M. B. Trzhaskovskaya, P. M. Davidson, and C. W. Nestor, Jr., "Evaluation of theoretical conversion coefficients using BrIcc," Nucl. Instrum. Methods Phys. Res. A **589**, 202 (2008), DOI: 10.1016/j.nima.2008.02.051.

[35] D. A. Brown *et al.*, "ENDF/B-VIII.0: The 8th major release of the nuclear reaction data library with CIELO-project cross sections, new standards and thermal scattering data," Nucl. Data Sheets **148**, 1 (2018), DOI: 10.1016/j.nds.2018.02.001.

[36] B. Acharya *et al.*, "Solar fusion III: New data and theory for hydrogen-burning stars," Rev. Mod. Phys. **97**, 035002 (2025), DOI: 10.1103/8lm7-gs18.

[37] S. N. Ghoshal, "An experimental verification of the theory of compound nucleus," Phys. Rev. **80**, 939 (1950), DOI: 10.1103/PhysRev.80.939.

[38] D. Adhikari *et al.* (PREX Collaboration), "Accurate determination of the neutron skin thickness of ^{208}Pb through parity-violation in electron scattering," Phys. Rev. Lett. **126**, 172502 (2021), DOI: 10.1103/PhysRevLett.126.172502.

[39] B. T. Reed, F. J. Fattoyev, C. J. Horowitz, and J. Piekarewicz, "Implications of PREX-II on the equation of state of neutron-rich matter," Phys. Rev. Lett. **126**, 172503 (2021), DOI: 10.1103/PhysRevLett.126.172503.

[40] B. Hu *et al.*, "Ab initio predictions link the neutron skin of ^{208}Pb to nuclear forces," Nature Phys. **18**, 1196 (2022), DOI: 10.1038/s41567-022-01715-8.

[41] E. Epelbaum, H.-W. Hammer, and U.-G. Meißner, "Modern theory of nuclear forces," Rev. Mod. Phys. **81**, 1773 (2009), DOI: 10.1103/RevModPhys.81.1773.

[42] H.-W. Hammer, S. König, and U. van Kolck, "Nuclear effective field theory: Status and perspectives," Rev. Mod. Phys. **92**, 025004 (2020), DOI: 10.1103/RevModPhys.92.025004.

[43] T. Otsuka, A. Gade, O. Sorlin, T. Suzuki, and Y. Utsuno, "Evolution of shell structure in exotic nuclei," Rev. Mod. Phys. **92**, 015002 (2020), DOI: 10.1103/RevModPhys.92.015002.

[44] H. Hergert, S. K. Bogner, T. D. Morris, A. Schwenk, and K. Tsukiyama, "The in-medium similarity renormalization group: A novel ab initio method for nuclei," Phys. Rep. **621**, 165 (2016), DOI: 10.1016/j.physrep.2015.12.007.

[45] J. M. Lattimer and M. Prakash, "The equation of state of hot, dense matter and neutron stars," Phys. Rep. **621**, 127 (2016), DOI: 10.1016/j.physrep.2015.12.005.

[46] J. M. Lattimer, "Neutron stars and the nuclear matter equation of state," Annu. Rev. Nucl. Part. Sci. **71**, 433 (2021), DOI: 10.1146/annurev-nucl-102419-124827.

[47] B. P. Abbott *et al.* (LIGO Scientific Collaboration and Virgo Collaboration), "GW170817: Observation of gravitational waves from a binary neutron star inspiral," Phys. Rev. Lett. **119**, 161101 (2017), DOI: 10.1103/PhysRevLett.119.161101.

[48] M. J. Dolinski, A. W. P. Poon, and W. Rodejohann, "Neutrinoless double-beta decay: Status and prospects," Annu. Rev. Nucl. Part. Sci. **69**, 219 (2019), DOI: 10.1146/annurev-nucl-101918-023407.

[49] M. Agostini, G. Benato, J. A. Detwiler, J. Menéndez, and F. Vissani, "Toward the discovery of matter creation with neutrinoless $\beta\beta$ decay," Rev. Mod. Phys. **95**, 025002 (2023), DOI: 10.1103/RevModPhys.95.025002.

[50] P. Gysbers *et al.*, "Discrepancy between experimental and theoretical β-decay rates resolved from first principles," Nature Phys. **15**, 428 (2019), DOI: 10.1038/s41567-019-0450-7.

[51] H. L. Crawford, K. Fossez, S. König, and A. Spyrou, "A vision for the science of rare isotopes," Annu. Rev. Nucl. Part. Sci. **74**, 141 (2024), DOI: 10.1146/annurev-nucl-121423-091501.

[52] Nuclear Science Advisory Committee, *A New Era of Discovery: The 2023 Long Range Plan for Nuclear Science*, U.S. Department of Energy and National Science Foundation (2023), `https://nuclearsciencefuture.org/`.

[53] S. A. Giuliani, Z. Matheson, W. Nazarewicz, E. Olsen, P.-G. Reinhard, J. Sadhukhan, B. Schuetrumpf, N. Schunck, and P. Schwerdtfeger, "Colloquium: Superheavy elements: Oganesson and beyond," Rev. Mod. Phys. **91**, 011001 (2019), DOI: 10.1103/RevModPhys.91.011001.

[54] N. Schunck and D. Regnier, "Theory of nuclear fission," Prog. Part. Nucl. Phys. **125**, 103963 (2022), DOI: 10.1016/j.ppnp.2022.103963.

[55] I. Counts, J. Hur, D. P. L. Aude Craik, H. Jeon, C. Leung, J. C. Berengut, A. Geddes, A. Kawasaki, W. Jhe, and V. Vuletić, "Evidence for nonlinear isotope shift in Yb^+ search for new boson," Phys. Rev. Lett. **125**, 123002 (2020), DOI: 10.1103/PhysRevLett.125.123002.

[56] I. Angeli and K. P. Marinova, "Table of experimental nuclear ground state charge radii: An update," At. Data Nucl. Data Tables **99**, 69 (2013), DOI: 10.1016/j.adt.2011.12.006.

[57] S. Kraemer *et al.*, "Observation of the radiative decay of the ^{229}Th nuclear clock isomer," Nature **617**, 706 (2023), DOI: 10.1038/s41586-023-05894-z.